Unravelling a mechanism of action of a cecropin A-melittin hybrid antimicrobial peptide – the induced formation of multilamellar lipid stacks

Tânia Silva [†,‡,⁑,¶], Bárbara Claro [†], Bruno F. B. Silva [¥], Nuno Vale [§], Paula Gomes [⊥], Maria Salomé Gomes [‡,⁑,¶], Sérgio S. Funari [ǂ], José Teixeira [#], Daniela Uhríková [+,], Margarida Bastos [†,*]*

[†] CIQ-UP – Centro de Investigação em Química, Departamento de Química e Bioquímica, Faculdade de Ciências, Universidade do Porto, Porto, Portugal;

[‡] i3S - Instituto de Investigação e Inovação em Saúde, Universidade do Porto, Porto, Portugal;

[⁑] IBMC – Instituto de Biologia Molecular e Celular, Universidade do Porto, Porto, Portugal;

[¶] ICBAS – Instituto de Ciências Biomédicas Abel Salazar, Universidade do Porto, Porto, Portugal;

[¥] INL – International Iberian Nanotechnology Laboratory, Braga, Portugal;

[§] UCIBIO/REQUIMTE, Laboratório de Farmacologia, Departamento de Ciências do Medicamento, Faculdade de Farmácia, Universidade do Porto, Porto, Portugal;

[⊥] LAQV/REQUIMTE, Departamento de Química e Bioquímica, Faculdade de Ciências, Universidade do Porto, Porto, Portugal;

[ǂ] HASYLAB, DESY, Hamburg, Germany;

[#] Laboratoire Léon Brillouin (CEA-CNRS), CEA Saclay, France;

[+] Faculty of Pharmacy, Comenius University in Bratislava, Bratislava, Slovak Republic.

KEYWORDS: Antimicrobial peptides; cecropin A; melittin; model membrane; calorimetry; X-ray diffraction; neutron scattering

ABSTRACT: The understanding of the mechanism of action of antimicrobial peptides is fundamental for the development of new and more active antibiotics. In present work, we use a wide range of techniques (SANS, SAXD, DSC, ITC, CD, confocal and electron microscopy) in order to fully characterize the interaction of a cecropin A-melittin hybrid antimicrobial peptide, CA(1-7)M(2-9), of known antimicrobial activity, with a bacterial model membrane of POPE/POPG, in an effort to unravel its mechanism of action. We found that CA(1-7)M(2-9) disrupts the vesicles inducing membrane condensation, forming an 'onion-like' structure of multilamellar stacks, held together by the intercalated peptides. SANS and SAXD revealed changes induced by the peptide in the lipid bilayer thickness and the bilayer stiffening, in a tightly packed liquid-crystalline lamellar phase. The analysis of the observed abrupt changes in the repeat distance upon the phase transition to the gel state suggests the formation of a L_{γ} phase. To the extent of our knowledge this is the first time that the L_{γ} phase is identified as a part of the mechanism of action of antimicrobial peptides. The energetics of interaction depends on temperature, and ITC results indicate that CA(1-7)M(2-9) interacts with the outer leaflet. This further supports the idea of a surface interaction that leads to membrane condensation and not to pore formation. As a result, we propose that this peptide exerts its antimicrobial action against bacteria through extensive membrane disruption that leads to cell death.

Introduction

Antimicrobial resistance is increasing rapidly, being one of the world's major health problems. Unfortunately, this is not being accompanied by the discovery of truly new drugs, but only 2nd and 3rd generation antibiotics.[1-2] Nevertheless, intensive research exists aiming at the development of alternatives to the existing drugs. Among others, antimicrobial peptides (AMP) are being extensively studied, as a new antibiotic paradigm. These diverse group of compounds are widespread in nature as part of the innate immune system of almost all living organisms.[3] They are active against several pathogens, such as viruses, protozoa, bacteria and fungi, acting on the pathogens' membrane, intracellular targets (*e.g.* proteins, nucleic acids), and/or through immunomodulation.[4-5] This capacity of attacking in multiple fronts enables them to evade resistance more easily than conventional drugs.[4] Several strategies have been employed to optimize the antimicrobial properties of these compounds with the main goal of decreasing their cytotoxicity towards host cells while maintaining or increasing their activity against pathogens. Another important goal is to attain a high selectivity, as of AMP with the smallest possible number of amino acids.[6]

One peptide improvement strategy that has been successfully used is hybridization, where parts of different peptides are combined into one molecule in order to optimize their individual characteristics.[7] Cecropin A-melittin hybrid peptides are one of the best examples of successful hybridization in the AMP field, first synthesized by Boman, *et al.* in 1989.[8] They are composed of the cationic region of cecropin A and the hydrophobic and non-hemolytic region of melittin. These hybrids have better antimicrobial properties than the parental compounds, with an improvement in the activity of cecropin A towards pathogens, together with a significant decrease in the hemolytic properties of melittin.[8-10] Their activity has been extensively studied, both on model membranes and on pathogens, and their mechanism of action is thought to rely on membrane disruption due to the formation of toroidal pores and/or detergent-like action.[10-20] Nevertheless, the antimicrobial peptide's mechanism(s) of action remain to be demonstrated, and can vary depending on membrane composition. Model membranes are extremelly helpful for a

detailed study of the different variables at stake, and can thus provide very insightful information on AMP mechanism of action and as such contribute to the development of more potent and less toxic antimicrobial peptides.

In present work we extensively characterize CAM's interaction with model membranes of 1-palmitoyl-2-oleoyl-*sn*-glycero-3-phosphoethanolamine and 1-palmitoyl-2-oleoyl-*sn*-glycero-3-phospho-(1'-*rac*-glycerol) (POPE/POPG 3:1 (mol/mol)), a good model for bacterial membranes, as they are the main lipids in several bacteria's membrane [21] in an attempt to ascertain its mechanism of action. The effect of the peptide is assessed by Small-Angle Neutron Scattering (SANS), Small-angle X-ray Diffraction (SAXD), Differential Scanning Calorimetry (DSC), Isothermal Titration Calorimetry (ITC), Circular Dichroism (CD) and microscopy techniques.

Our results show that CAM interacts strongly with the negatively charged model membrane system, and induces lipid segregation and extensive vesicle disruption, forming a condensed 'onion-like' multilamellar structure with the peptide intercalated within the lamellae. Further and most interestingly, results at temperatures below the fluid phase indicate that the peptide induces formation of a new phase, L_{γ}, with a significantly different spatial arrangement of POPE and POPG.

Material and Methods

Peptides

CA(1–7)M(2–9) or CAM (KWKLFKKIGAVLKVL-NH_2) was synthesized, purified, and characterized as described previously.[22] Peptide stock solutions were prepared in Phosphate Buffered Saline (PBS, 9.3 mM, 150 mM NaCl, pH 7.4) or HEPES buffer (HEPES 10 mM, 150 mM NaCl, pH=7.0) and stored at -20 °C until use.

Preparation of Liposomes

Oligolamellar (non-extruded) (OLVs), and unilamellar (extruded) vesicles (LUVs) of 1-palmitoyl-2-oleoyl-*sn*-glycero-3-phosphoethanolamine (POPE) and 1-palmitoyl-2-oleoyl-*sn*-glycero-3-phospho-(1'-

rac-glycerol) (POPG) (Avanti Polar Lipids, Alabama, USA) in a proportion 3:1 (mol/mol) were prepared as described before.[23]

Small-angle neutron scattering

Neutron scattering experiments were performed at the PAXY spectrometer located at the G2 cold neutron guide of the Orphée reactor (Laboratoire Léon Brillouin, Saclay, France). The sample to detector distance was 2.75 m and the neutron wave-length was λ=6 Å ($\Delta\lambda/\lambda$=10 %) covering the scattering vector range 0.015-0.22 $Å^{-1}$. The temperature of the samples was set to 36 °C ±0.1 °C. The acquisition time for each sample was 30 min. The normalized SANS intensity *I(q)* as a function of the scattering vector *q* was obtained using Pasinet data treatment software provided by LLB. All spectra were corrected for incoherent background. Detailed description of sample preparation and handling can be found in supplementary material.

Small-angle X-ray Diffraction

Small-angle X-ray diffraction (SAXD) experiments were performed at the synchrotron soft condensed matter beamline A2 in HASYLAB at Deutsches Elektronen Synchrotron (DESY), Hamburg, Germany, using a monochromatic radiation of λ=1.5 Å wavelength. Diffractograms were taken at selected temperatures, with 5 min of sample equilibration time. Temperature scans were performed at a scan rate 1 °C/min, where diffractograms were recorded for 10 s every minute. The evacuated double-focusing camera was equipped with a 2D MarCCD detector or a linear position sensitive detector for SAXD. The raw data were normalized against the incident beam intensity. The SAXD patterns were calibrated using Ag behenate [24] or rat tailcollagen [25]. Each Bragg diffraction peak was fitted by Lorentzian above a linear background. Detailed description of sample preparation and handling can be found in supplementary material.

Differential Scanning Calorimetry

Differential scanning calorimetry (DSC) was performed in a MicroCal VP-DSC microcalorimeter from Malvern (Worcestershire, UK). The results provided here refer to the third heating scan. The sample mixtures were prepared immediately before the DSC run, by adding the desired amount of peptide stock solution to the OLVs suspension. In the case of pure liposome suspension, the temperature (T_m) and the enthalphy ($\Delta_{trans}H$) of transition were calculated by integration of the heat capacity versus temperature curve. In the case of peptide/lipid mixtures the curves were decomposed into two transitions that clearly show up in the global profile. In both cases the total $\Delta_{trans}H$ is reported, together with the % of total area ($100*A_i/A_{tot}$) represented by each peak for the peptide/lipid mixtures, as no correct $\Delta_{trans}H$ assignment can be made to each of them. The respective T_m and half width at half height (HWHH) are also provided in each case. Detailed description of sample preparation and blank experiments are provided in the supplementary material.

Isothermal Titration Calorimetry

Isothermal Titration Calorimetry (ITC) measurements were performed in a MicroCal VP-ITC microcalorimeter from Malvern (Worcestershire, UK). Lipid-into-peptide titrations were performed by injecting 3-4 μL aliquots of POPE/POPG 3:1 LUVs (15 or 30 mM) into the calorimeter cell containing the peptide at concentrations between 10 and 25 μM. Titrations were performed at 5, 17 and 30 °C. Inverse titration experiments (250 μM of peptide titrated into 30 mM of liposome suspension), as well as dilution experiments of LUVs into buffer were also performed. ITC data analysis for the experiments in the fluid phase (30 °C) was made by use of two approaches. First, the raw data was imported to the NITPIC software [26] and the obtained datasets were analyzed by a nonlinear least-squares fitting using a Microsoft EXCEL spreadsheet (Microsoft, Redmond,WA) kindly provided by Prof. Sandro Keller, Kaiserlautern, Germany.[27] In a second approach, the raw data was imported to the AFFINImeter software and analyzed using an *independent sites* model (https://www.affinimeter.com/).

Circular Dichroism

Circular Dichroism (CD) experiments were carried out in a Jasco J-815 spectropolarimeter (JASCO Corporation, Tokyo) equipped with a rectangular cell, path length of 1 mm. Scans were performed between 190 – 250 nm, with a scan speed of 100 nm/min, digital integration time (DIT) 1 second, data pitch 0.1 nm and bandwidth 1.0 nm. The measurements were performed in PBS (9.3 mM, 150 mM NaF, pH 7.4). The peptide solution and liposome suspension (LUVs) were mixed just prior to each measurement, incubated at 35 °C for 30 min and measurements were performed thereafter at the same temperature. Each spectrum is the average of twelve accumulations. After blank correction (spectra of pure liposomes), the observed ellipticity was converted to a mean residue molar ellipticity (θ) ($deg cm^2 dmol^{-1}$), based on the total amount of peptide in the mixture, considering all amino acids.

Confocal Microscopy

OLVs of POPE/POPG 3:1 (mol/mol) were prepared as stated above with the addition of 0.3% Texas Red®-1,2-dihexadecanoyl-*sn*-glycero-3-phosphoethanolamine (Texas Red®-DHPE) (Molecular Probes). Mixtures of peptide solution and liposome suspension (OLVs) were prepared at different peptide-to-lipid (P:L) molar ratios, and were incubated for 30 min at 35 °C. The samples were observed and photographed in a Laser Scanning Confocal Microscope Leica SP2 AOBS SE (Leica Microsystems, Germany).

Electron Microscopy

Negative staining electron microscopy was performed on samples of LUVs of POPE/POPG 3:1 (mol/mol) and on mixtures of CAM with POPE/POPG 3:1 at different peptide-to-lipid (P:L) ratios and temperatures (detailed sample preparation can be found in the supplementary material). The samples were observed and photographed in a Jeol JEM-1400 transmission electron microscope (TEM).

Results and Discussion

Small-angle neutron scattering

158 Neutron scattered intensity, *I(q),* is measured in function of the momentum exchange *q,* which depends
159 on the wavelength λ of the incident neutron beam and on the scattering angle 2θ:

160 $q=4\pi\sin(\theta)/\lambda$

161 Figure 1 (inset) shows *I(q)* of POPE/POPG 3:1 (mol/mol) dispersion of vesicles prepared by extrusion.
162 The broad peak ($0.05 \leq q \leq 0.11$ Å^{-1}) reflects the presence of a small fraction of oligo or multilamellar
163 vesicles. Indeed, in spite of careful preparation and thorough extrusion, unilamellar POPE/POPG vesicles
164 gradually aggregate. Similarly, low stability over time of DPPE/DPPG unilamellar vesicles was recently
165 reported.[28]

166 The paracrystal lamellar model [29] fits well the data, as shown by the full line in Figure 1 (inset). Fitting
167 processed with SasView software[30] yields values for number, periodicity and distribution of layers in a
168 single cluster. The model is sensitive to detect structural changes in vesicles dispersions, particularly when
169 low fraction of oligo-lamellar vesicles contaminates a dispersion of unilamellar vesicles, as we shown
170 recently.[31] The scattering length density per unit mass of the solute is calculated from known POPE/POPG
171 molar ratio using the appropriate molecular volumes and molecular weights.[32-33] The ideal model
172 scattering curve is smeared by the instrumental resolution which is calculated for each *q* value. In average,
173 $\Delta q/q$ ~10 %.

174 The best fit corresponds to a mixture of uni- and multilamellar vesicles consisting of up to 8 bilayers
175 with a spacing fluctuating in the range ~ 57 - 97 Å. The lipid bilayer thickness is δ= 39.4±0.2 Å. Previous
176 SAXS studies of the same system showed that the number of layers is of the order of 3-5, independent of
177 POPG content,[34] similarly to our results. As well, the obtained lipid bilayer thickness agrees with
178 published data. Molecular dynamic simulations predicts a lipid bilayer thickness equal to 40.1±0.1 Å for
179 POPE/POPG (5.3:1) (mol/mol).[35] Kučerka *et al.* [32, 36] reported lipid bilayer thicknesses equal to δ=40.5
180 Å (at 35 °C) and δ=36.3 – 38.5 Å (at 30 °C), for POPE and POPG, respectively.

Figure 1 shows *I(q)* of CAM-POPE/POPG mixtures at three selected molar ratios and 36 °C. When the OLV dispersions are mixed with the CAM peptide, a fine white precipitate spontaneously forms, suggesting massive aggregation and condensation of the lipid bilayers induced by the peptide. Microscopy images illustrate well these massive structural changes, as documented below (figures 9 and 10).

The peak observed in the SANS curves at q ~ 0.128 $Å^{-1}$ reflects these structural changes in the dispersion, due to peptide interaction with POPE/POPG bilayer, since the lowest studied molar ratio, P:L=1:25. Data treatment has confirmed that the paracrystal lamellar model applied for weakly interacting bilayers (like in POPE/POPG vesicles) is not adequate to the system containing the peptide. Therefore, we use a model proposed by Nallet *et al.* [37] for a lyotropic lamellar phase where a random distribution of clusters in solution is assumed. The calculation is based on Caillé's model [38] that takes into account a combination of two models for the form and the structure factor. In this model, *I(q)* is given by

$$I(q)=2\pi\frac{P(q)S(q)}{\delta q^2} \quad (1)$$

The form factor is

$$P(q)=\frac{2\Delta\rho^2}{q^2}\left(1-\cos(q\delta)\right) \quad (2)$$

where $\Delta\rho$ is the contrast between the coherent neutron-scattering length densities (SLD) of bilayer and solvent. The structure factor S(q) is given by

$$S(q)=1+2.\sum_1^{N-1}\left(1-\frac{n}{N}\right)\cos(qdn)\exp\left(-\frac{2q^2d^2\alpha(n)}{2}\right) \quad (3)$$

where N is the number of lamellae in a cluster and d is the period of the stacking. $\alpha(n)$ is a correlation function for undulating lamellae expressed by

$$\alpha(n)=\frac{\eta_{cp}}{4\pi^2}\left(ln(\pi n)+\gamma_E\right) \quad (4)$$

with the Euler's constant γ_E = 0.5772157 and the Caillé parameter η_{cp} defined in terms of the elastic constants of the layers, B (bulk modulus for layer compression) and K (bulk modulus for layer curvature) by

$$\eta_{cp}=\frac{q_1^2\, k_B T}{8\pi\sqrt{KB}} \quad (5)$$

where q_1 is the position of the first order Bragg peak, k_B is the Boltzmann constant and T the temperature. From η_{cp} we can calculate the fluctuations in bilayer separation, $\Delta\sigma^2=\eta_{cp}\,.d^2/\pi^2$ [39]. *I(q)* data are compared to the theoretical prediction using SasView fitting software.[30] Smearing due to instrumental resolution is taken into account. The lamellar spacing d is taken from the first order Bragg-peak position as $d=2\pi/q_1$. The scattering contrast $\Delta\rho$ is calculated from the chemical composition. Consequently, the independent fitting parameters are limited to four: the number N of bilayers, the thickness of the lipid bilayer δ, the Caillé parameter η_{cp}, and the amplitude. Full lines in Figure 1 represent the best fits; corresponding parameters are in Table 1. They show that some properties of the bilayer are significantly affected by the presence of CAM. The peptide is initially attracted to the vesicle's surface (electrostatic attraction) and induces partial membrane segregation (due to preference for POPG), together with the formation of 'onion-like' structures with intercalated peptide, and a large number (N) of stacked bilayers that increases with peptide content.

Table 1. Structural parameters of POPE/POPG 3:1 (mol/mol) vesicles and CAM-POPE/POPG mixtures at 36 °C obtained from the analysis of the SANS data.

Sample	P:L / mol/mol	d / Å	δ / Å	N	η_{cp}	$(KB)^{1/2}$ / N.m^{-1}	$\Delta\sigma$ / Å
POPE/POPG	-	~ 57 - 97	39.4±0.2	~1 - 8	-	-	-
CAM-POPE/POPG	1:25	50.5±0.1	41.6±0.1	18	0.27±0.02	(0.97±0.08)x10^{-3}	8.4±0.3
CAM-POPE/POPG	1:17	49.8±0.1	40.5±0.1	24	0.15±0.03	(1.80±0.40)x10^{-3}	6.1±0.6
CAM-POPE/POPG	1:10	49.6±0.1	38.7±0.1	42	0.11±0.03	(2.48±0.80)x10^{-3}	5.2±0.7

227 d- repeat distance; δ-bilayer thickness; N- number of stacked bilayers; η_{cp} - Caillé parameter; B - bulk
228 modulus for layer compression and K -bulk modulus for layer curvature; $\Delta\sigma$- fluctuations in bilayer
229 separation.

230

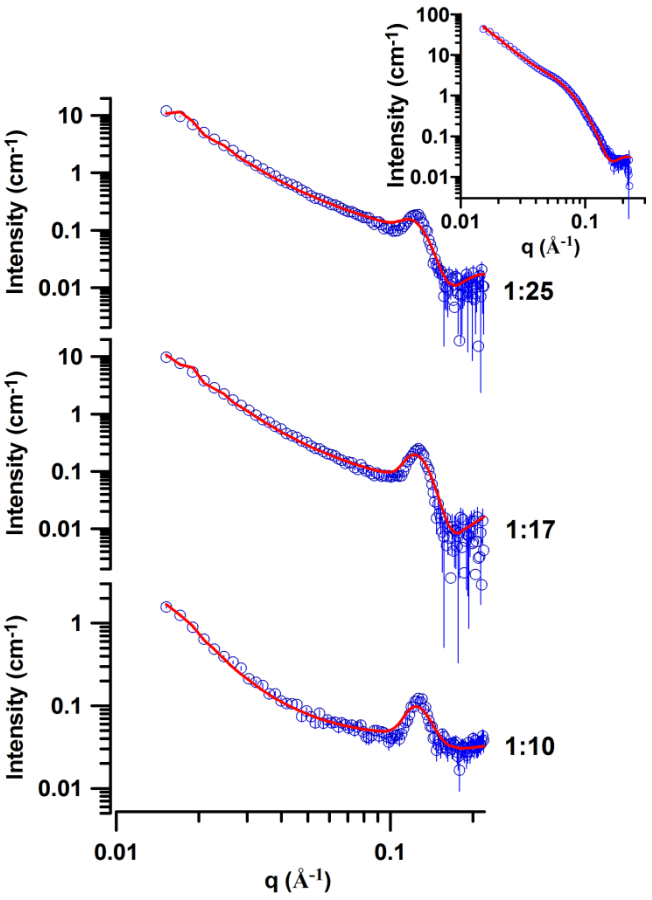

231

232

Figure 1. SANS curves of CAM-POPE/POPG mixtures at peptide to lipid molar ratios P:L=1:25; 1:17; and 1:10 at 36 °C; inset: SANS curve of POPE/POPG 3:1 (LUVs) dispersion at 36 °C. Full lines represent fitting curves.

The repeat distance *d* decreases with increasing amount of CAM. Changes in the lipid bilayer thickness δ are also detected. This value initially slightly increases (~+ 2.2 Å) at P:L 1:25, and then decreases until P:L 1:10 (~ - 0.7 Å) as compared to the value δ = 39.4 Å observed for POPE/POPG vesicles. These changes in bilayer thickness with P:L molar ratio can be related to the progressive neutralization of the membrane charge by the peptide. Both effects (membrane thickening and thinning due to peptide interactions) are documented in literature. Pabst *et al.* [40] observed a similar increase of lipid bilayer thickness up to ~ 0.9 – 2 Å due to antimicrobial peptide (peptidyl-glycylleucine-carboxyamide) interaction with dimyristoyl– and dipalmitoylphosphatidylglycerol membrane (DMPG, DPPG) at P:L 1:25, similar to the ratio where we also observe the same effect. Membrane thinning (~ 1.5 - 3 Å) was reported in the melittin/neutral phospholipid (POPC and diC22:1PC) system when oriented bilayers of the peptide/lipid mixture were deposited in a quartz surface and hydrated to 98 % RH.[41] The Caillé parameter is a measure of the average fluctuation in bilayer separation, expressed through $\Delta\sigma$. η_{cp} and *KB* (Table 1) indicate the stiffening of the lipid bilayer due to its interaction with CAM. Increasing amounts of peptide increase the lipid bilayer rigidity and damps its fluctuation, as manifested by increasing values of *KB* and decreasing values of $\Delta\sigma$ (Table 1). As mentioned, the peptide is attracted electrostatically to the membrane surface (see also below DSC and ITC results) where it takes a α-helix secondary structure (see below CD results), adsorbing parallel to the membrane surface. The decrease in bending modulus of the bilayers was reported previously for this type of peptide-membrane arrangement.[42-44] Stiffening of the membrane due to the interaction with the antimicrobial peptide $rBPI_{21}$ was also reported by Domingues *et al.*[45]

Small-angle X-ray Diffraction

Typical diffractograms are plotted in Figure 2. In the liquid-crystalline state (L_α phase) of the pure lipid mixture, at 30 °C, POPE/POPG 3:1 (mol/mol) vesicles show a broad peak with two not well resolved maxima (Figure 2A). The increase in water thickness between lamellae and their fluctuations give rise to disorder in the relative positions of the unit cells, resulting in broadening of the diffraction peaks, an effect that increases with temperature.[46] The pattern characterizes a system with poor long range order, as expected for OLV vesicles with negatively charged surface due to the presence of POPG. When the peptide is added to the POPE/POPG vesicles, SAXD confirms the presence of a well-organized lamellar phase. For comparison, the diffraction patterns at the bottom correspond to POPE multilamellar vesicles in liquid-crystalline (at 30 °C) and gel (at 10 °C) phases (Figure 2A, B). In figure 3A we plotted the repeat distance $d = 2\pi/q_1$ where q_1 is the position of the first order peak, as a function of P:L molar ratio, together with the repeat distance of POPE (dashed line in Figure 3A; d_{POPE}=53.7±0.1 Å at 30 °C). The empty symbols in Figure 3A show the repeat distances derived from SANS experiments at 36 °C (Table 1), whereas full diamonds and triangles show the repeat distance at 30 and 40 °C, respectively, obtained by SAXD. The observed small discrepancies in d values obtained by SANS and SAXD result from differences in sample preparation (*e.g.* use of deuterated water in SANS) and their history prior to measurements (we started with LUVs in the case of SANS measurements and OLVs in the case of SAXD measurements). At 30 °C, where the system is in L_α phase, the repeat distance $d_{CAM\text{-}POPE/POPG}$ decreases with increasing P:L ratio (Figure 3A, full diamonds). This can be attributed to POPE/POPG surface charge compensation, due to interaction with the peptide. A similar effect was reported for the interaction of cationic liposomes with polyelectrolytes of opposite charges, like DNA.[47-49] The increase in temperature enhances the effect, as shown in the values for 40 °C (Figure 3A, full triangles). At 50 °C (data not shown), $d_{CAM\text{-}POPE/POPG}$=49 Å for P:L=1:7, while for zwitterionic POPE we found d_{POPE}=51.6 Å. The polar headgroup of phosphatidylethanolamines is less hydrophilic than phosphatidylcholines, as PE headgroups tend to form hydrogen bonds with each other rather than with water, which is not possible for PC. This

leads to a smaller water content between PE bilayers. The repeat distance of POPE decreases at high temperature, and the lipid bilayer thickness decreases as well.[32] We attribute the observed decrease in $d_{CAM\text{-}POPE/POPG}$ at higher temperature to two effects: the decrease of the lipid bilayer thickness due to its thermal lateral expansion, and the expulsion of water from the interlamellar space. We should refer that the mixture CAM-POPE/POPG keeps the lamellar structure even when heating the samples above 70 °C when POPE alone forms an inverted hexagonal phase.

The situation is more puzzling when the system is cooled below ~ 20 °C, and POPE is in the gel state. The diffractograms obtained at 10 °C are plotted in Figure 2B. Hydrated POPE alone forms multilamellar vesicles, with a repeat distance d_{POPE} ~ 63 Å. However, the lamellar system of POPE/POPG swells, due to negative surface charge imposed by POPG. We determined the repeat distance of POPE/POPG 3:1 (mol/mol) at 10 °C to be $d_{POPE/POPG}$=105.6±2.1 Å. Pozo Navas *et al.* [34] reported swelling of POPE/POPG mixture with increasing POPG content, showing periodicities up to 132 Å in the gel phase. Surprisingly, the lamellar phase formed due to CAM interaction with POPE/POPG at low temperatures shows also a large periodicity for all studied molar ratios. However, in comparison with the pure POPE/POPG vesicles, the diffractograms show a much more organized lamellar structure, and the width of the peaks decreases with increasing peptide content (expressed through P:L molar ratio) (Figure 2B). In addition, we observe a small peak (marked by the arrow in Fig. 2B and C) at q ~ 0.097 Å^{-1} (d ~ 64.8 Å) clearly resolved in diffractograms of the mixtures with higher peptide contents (P:L=1:10 and 1:7).

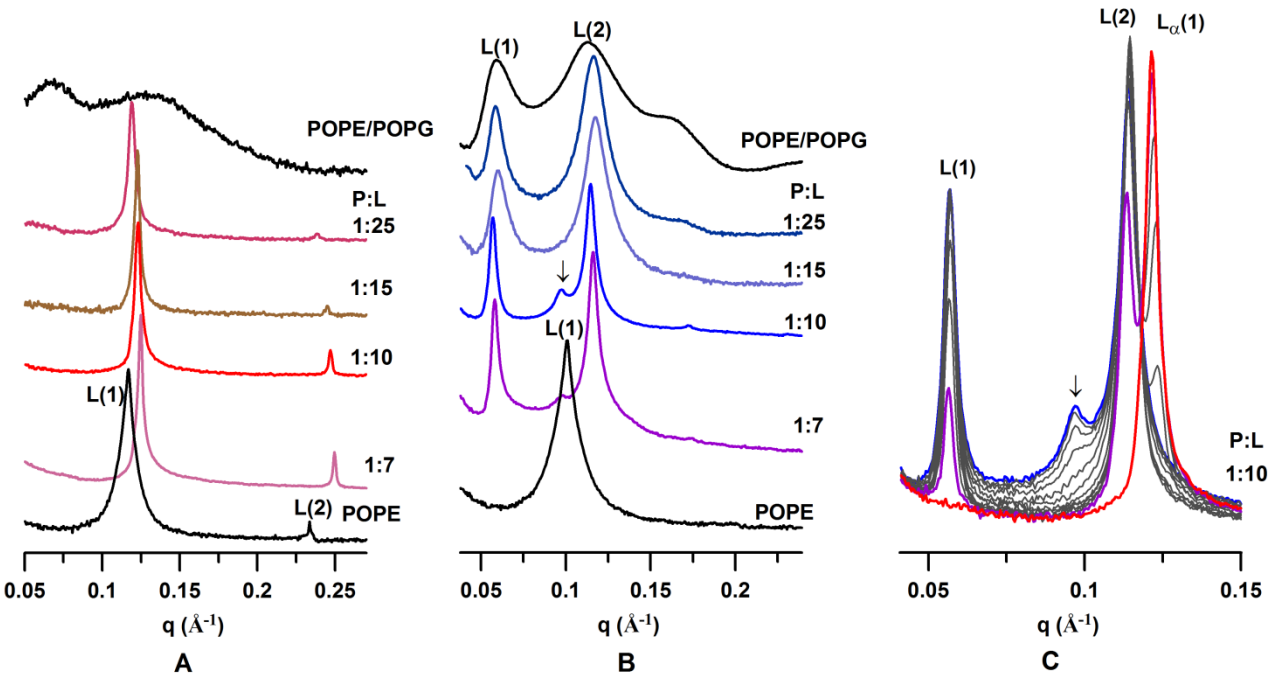

300

301

302 **Figure 2.** SAXD patterns of multilamellar (OLVs) POPE, POPE/POPG and CAM-POPE/POPG mixtures
303 in (A) a liquid-crystalline state at 30 °C; (B) gel state at 10 °C; (C) diffractograms of CAM-POPE/POPG
304 at P:L=1:10 at temperatures from 10 °C (blue line) to 24 °C (red line), in steps of 1 °C.

305 In Figure 3B the repeat distances for the lipid system and peptide mixtures are plotted for 10 and 20 °C
306 (Figure 3B, full circles and full squares, respectively), as a function of P:L ratio. We can see that the lipid
307 system swells ($d_{POPE/POPG}$ ~ 120 Å) with increasing temperature. At odds with the liquid-crystalline state,
308 the repeat distance $d_{CAM\text{-}POPE/POPG}$ at 10 °C slightly increases with increasing peptide content (Figure 3B,
309 full circles). At 20 °C, close to the phase transition (T_m=22.2 °C for POPE/POPG 3:1 (mol/mol), see also
310 DSC results) (Figure 3B, full squares) the repeat distance $d_{CAM\text{-}POPE/POPG}$ decreases significantly with
311 increase in the P:L ratio. Moreover, the repeat distances of the mixtures for the highest CAM contents
312 (P:L=1:10 and 1:7) coincide, in spite of a temperature increase of 10 °C ($d_{POPE/POPG}$ ~ 110 Å), indicating
313 a "tightly packed system".

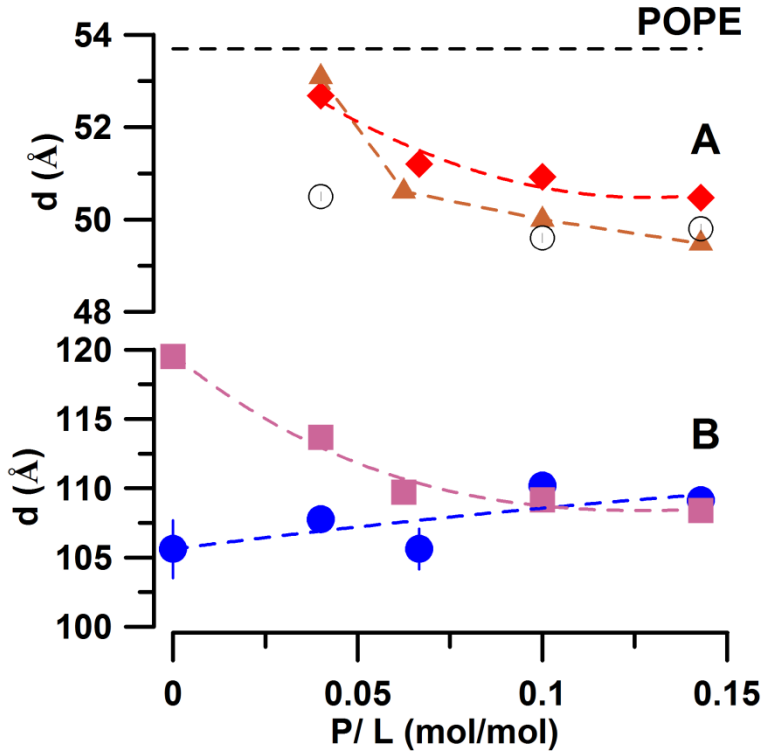

Figure 3. Repeat distances of lamellar phases formed by CAM-POPE/POPG (OLVs) derived from SAXD: (A) in a liquid-crystalline state at 30 (full diamond) and 40 °C (full triangle), d derived from SANS at 36 °C (empty circles), d_{POPE} at 40 °C (horizontal dashed line); (B) in a gel state at 10 (full circles) and 20 °C (full squares). The P:L ratios in the text are here represented as P/L fractions.

In summary, CAM-POPE/POPG 3:1 (mol/mol) in the liquid-crystalline state shows a lamellar phase with repeat distance ~ 51 Å that abruptly increases to more than twice (~ 110 Å) when the system is cooled to a gel state. These changes are highly reversible in repeated heating - cooling cycles of the samples in a temperature range of 10 – 80 °C (Figures S1 and S2). This peculiar behavior deserves a deeper analysis. Combining our SAXD and SANS results allow us to determine the average thickness of water layer (including the peptide) between the bilayers as $d_w = d - \delta = 10.3 \pm 1.2$ Å in L_α phase (at 30 to 40 °C). We did not perform SANS measurements of the system in a gel state, but Pozo Navas et al.[35] determined a

head-to-headgroup distance d_{HH}=45.6±0.2 Å for POPE/POPG bilayer in a gel state. The peptide binding does not affect the lipid bilayer thickness significantly (Table 1). We can thus get an approximate thickness of the water layer as $d_w \sim 110 - 46 = 64$ Å in a gel state of CAM-POPE/POPG. For zwitterionic lipids, the thickness d_w is the result of a balance between repulsive interbilayer interactions (steric, hydration and fluctuations) and attractive van der Waals forces,[46] and typically does not exceed ~ 15 Å in a gel state. However, the presence of uncompensated charges at the bilayer surface results in that the electrostatic repulsion between bilayers overcomes the van der Waals attraction, the inter-bilayer distance increases markedly, and the lamellar stacking is disordered. The observed SAXD patterns of POPE/POPG show broad, poorly resolved peaks that reflect such disorder in the relative positions of the unit cells. Surprisingly, CAM-POPE/POPG mixtures show a well ordered lamellar phase, with the width of the peaks decreasing with increasing amount of the peptide (Figure 2 B), similar to that observed for zwitterionic POPE in both gel and liquid-crystalline states. Indeed, the presence of the peptide dumps the bilayer fluctuations as follows from our simple analysis (Figure S3). Figure 2C shows structural changes of CAM-POPE/POPG when heating from 10 °C (blue line) to 24 °C (red line). Note that the periodicity of L_α phase is reduced to more than half as comparison to the one observed in the gel state. Moreover, the phase transition is rather narrow (< 5 °C). Such a marked swelling through the phase transition (d_w increases ~ 6 times), without any significant changes in the positional order of unit cells of a lamellar phase is difficult to ascribe to differences in the peptide adsorption to the membrane surface in gel and liquid-crystalline state, raising the question whether such a large interlamellar space (~ 64 Å) in the gel state of the system is filled with water and the peptide?

In literature, such abrupt changes in periodicity were reported within specific temperature ranges for mixtures formed by two (or more) lipids that include acyl chains in two different conformations: type α, in a liquid-crystalline state, and type β, in a gel state.[50-53] Heterogeneous chains usually segregate into regions with different conformation. A phase $L_{\alpha\beta}$ was described consisting of regularly stacked lipid

lamellae, each of them being a disordered mosaic of two types of domains - with the chains either in the α or in the β conformation. The repeat distance of such organization varies between the periodicity of a lamellar phase when the mixture is either in L_α or in L_β phase. [52] Another way of segregation was reported, where a lamellar phase consisting of two lipids in its unit cell is formed. [52-53]

There are two possible arrangements in this case: (i) two alternating bilayers exist, formed by one bilayer of type α (αα - two monolayers of α) and one of β (ββ - two monolayers of β), with the mirror plane located in the middle of the hydrocarbon region (abbreviated as L_γ phase - model A in Figure 4);[52] (ii) each lipid lamellae is formed by one monolayer of type α and one of type β, joined by their apolar faces (αβ), with the mirror plane located in the center of polar region (abbreviated as L_γ phase - model B in Figure 4).[52-53] The repeat distance of such complex double-bilayer lamellar phase is larger, *i.e.*, about twice the simple bilayer. The analysis of crystallographic data cannot discriminate the two possible structures of the L_γ phase.[52] A double lamellar phase L_γ (Figure 4, model A) was first reported in a system containing a protein from the myelin sheath, acidic phospholipids and sulphatides.[51] The double bilayer phase transformed into an ordinary bilayer phase at higher temperatures, involving chain melting. Gulik *et al*.[50] identified L_γ phase (Figure 4, model B) in a mixture of lipids of bovine lung surfactant. With increasing temperature and water content the L_γ is transformed into L_α phase. A double bilayer lamellar phase (model A) was also detected in a mixture of lysophospholipids and fatty acid.[54] Its structure was confirmed by simulations of the X-ray scattering pattern.

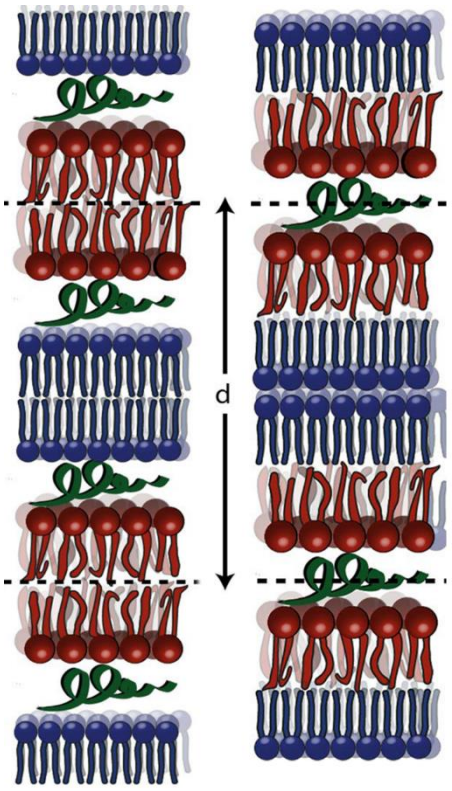

Figure 4. Representative models A and B of L_γ phase of CAM-POPE/POPG system. Blue - POPE, red - POPG, green – CAM.

In our system, the lipid mixture consists of POPE with gel to liquid-crystalline phase transition temperature T_m ~ 24.7 °C, and POPG with T_m ~ - 5.3 °C.[34] Thus in the studied temperature range 10 – 20 °C, the hydrophobic core of the mixture of POPE/POPG 3:1 (mol/mol) consists of acyl chains with both conformations: type β of POPE, and type α of POPG. Thermodynamically, the two lipids mix non-ideally.[34] We can assume that the positively charged CAM interacts preferentially with POPG, because of its negatively charged polar group and acyl chains in liquid-crystalline state enhancing peptide partition (type α). Thus CAM can trigger lipid segregation resulting in the formation of a L_γ phase. Due to the preference of CAM to POPG, we consider that our system assumes a L_γ phase in model B, as the peptide will be in close contact with the POPG headgroups (Figure 4). Importantly, careful inspection of WAXD

patterns in the gel state indicates the formation of domains rich of POPE (Figure S4), and DSC data (below) also supports this finding.

At P:L=1:10, in a range of 10 to 23 °C, in addition to the peaks assigned to the L_γ phase (*L(1)* and *L(2)*), we observe a small peak (or more accurately a shoulder) at the left side of *L(2)* ($q \sim 0.097$ Å^{-1}, marked by an arrow in Figure 2B,C). Its intensity decreases with increasing temperature, and the peak merges in the background at ~ 15 °C. Concurrently, the intensity of *L(2)* increases with temperature up to the $L_\gamma \rightarrow L_\alpha$ phase transition. The periodicity associated to this extra peak is d=64.8 Å, a value slightly larger than the repeat distance of fully hydrated POPE (d=62.5 Å at 10 °C). SAXD shows clearly this additional periodicity at the two highest P:L molar ratios, and the phase was observed preferentially during the cooling process. At lower P:L ratios, the peak merges with *L(2)* and can be seen as an insignificant shoulder (Figures 2C and S2). However, its presence cannot be considered as accidental, as it was observed in independently prepared samples, even at different measuring periods. There are two possible interpretations: the peak can be attributed either to a packing defect of L_γ phase, or it reflects the presence of a new phase in the mixture when cooling the sample below ~ 15 °C. The systematic presence of the peak in successive heating-cooling scans supports the second possibility, *i.e.* the formation of a new phase at temperatures below ~ 15 °C, co-existing with the L_γ phase. As will be seen below in the DSC section, our DSC experiments confirm the presence of a new phase transition in the peptide/lipid system at $T_m \sim$ 14 °C for all P:L molar ratios. The present SAXD data, obtained at temperatures above 10 °C, do not allow explicit identification of the structural arrangement of CAM - POPE/POPG mixtures at low temperatures (<14 °C). A possible interpretation is that it can indicate the origin of another lamellar phase at low temperatures in this complex peptide/lipid system, but we cannot exclude an arrangement in a phase of higher symmetry due to compounds de-mixing.

Differential Scanning Calorimetry

405 The effect of CAM on the thermotropic lipid transition was evaluated on both POPE/POPG 3:1 OLVs
406 and LUVs, for different P:L ratios. Similar profiles were obtained, thus only the results for OLVs are
407 shown here. The peptide has a very strong effect on the lipid system (Figure 5). The lipid transition for
408 the pure POPE/POPG 3:1 (mol/mol) presents in both cases a profile that indicates non-ideal mixing
409 between the two lipids (non-symmetric transition with low cooperativity), which have widely different
410 transition temperatures, 24.7 °C for POPE and -5.3 °C for POPG.[34]
411
412 **Table 2.** Characterization of the phase transitions observed in DSC experiments with POPE/POPG 3:1
413 (mol/mol) OLVs and their mixtures with the CAM peptide at different P:L molar ratios. For each system,
414 T_m, ΔH and HWHH are provided. For CAM-POPE/POPG mixtures at different P:L ratios the areas of the
415 two peaks observed are also presented. The uncertainty in ΔH values is ±2 kJ.mol^{-1} and in T_m is ±0.3 °C.

P:L	ΔH / kJ.mol^{-1}	T_{m1} / °C	% total area (100*A_1/A_{tot})	$HWHH_1$ / °C	T_{m2} / °C	% total area (100*A_2/A_{tot})	$HWHH_2$ / °C
0	23	-	-	-	22.2	100	5.2
1:25	13	15.1	9	4.2	22.7	92	5.1
1:15	14	14.4	14	3.7	22.3	86	5.2
1:10	16	13.8	9	3.4	22.2	92	4.8
1:7	17	13.6	6	3.3	22.2	94	4.7

416 P:L - Peptide-to-lipid molar ratio; ΔH - total transition enthalpy; T_{mi} - transition temperature; HWHH -
417 half width at half height

418 Indeed, the transition is more cooperative in the case of OLVs when comparing to LUVs, due to higher
419 number of layers in the first case. We obtain a T_m = 22.2 °C in the case of POPE/POPG 3:1 OLVs (Table
420 2) and 19.1 °C for LUVs. The value for OLVs is in the range of the values reported for OLVs by Pozo
421 Navas *et al.*, (22.7 °C for x_{POPG}=0.18 and 20.6 °C for x_{POPG}=0.30).[34] Teixeira *et al.*[14] reported the value
422 20.4 °C for LUVs, similar to our results. As regarding the transition enthalpy, we obtain $\Delta_{trans}H$=23 kJmol^{-1}
423 [1] for OLVs and 24 kJmol^{-1} for LUVs, in very good agreement with Teixeira *et al*. value for LUVs, 22

kJmol^{-1} [14] as well with Pozo Navas *et al.* value for OLVs, (24.2 kJmol^{-1} for x_{POPG}=0.18 and 25.5 kJmol^{-1} for x_{POPG}=0.30),[34] considering that according to our experience $\Delta_{trans}H$ can vary within ± 2 kJmol^{-1} for the same sample conditions and different liposome preparations.

For the peptide/lipid mixtures, we can see that peptide addition induces a phase separation at all PL: ratios here reported, reflected in the appearance of a new peak at lower temperatures (Figure 5). We performed curve decomposition for all reported P:L ratios (see example in Figure S5), and the parameters and values retrieved are reported in Table 2. Curiously, the temperature of the main transition is almost invariant for all P:L ratios, both for OLVs and LUVs, ~22 °C. Further, a thinning effect is also apparent (see HWHH values), much more pronounced in the case of LUVs, consistent with an increase in lamellar stacking, reflecting the formation of 'onion-like' structures with intercalated peptide. According to the model suggested above in the SAXD section, we consider that this transition corresponds to the $L_\gamma \rightarrow L_\alpha$ phase.

The new transition observed at lower temperature is also in line with the SAXD findings, as it shows a T_m around 14-15 °C, varying only slightly in the case of OLVs, and significantly in the case of LUVs, where it starts at 19 °C for P:L 1:25 and stabilizes at 14 °C for the two highest P:L ratios. This new phase is clearly better defined at the highest P:L ratios, and the observed transition could be into either the L_γ phase or directly into the L_α phase at ~ 14-15 °C.

Finally, the total enthalpy (obtained from the area encompassing the two peaks) decreases significantly in presence of the peptide (Table 2), suggesting that the enthalpy changes in the presence of peptide are lower than the enthalpy change for the pure POPE/POPG 3:1 lipid system, particularly the $L_\gamma \rightarrow L_\alpha$ phase transition, as it is the more significant part of the total area.

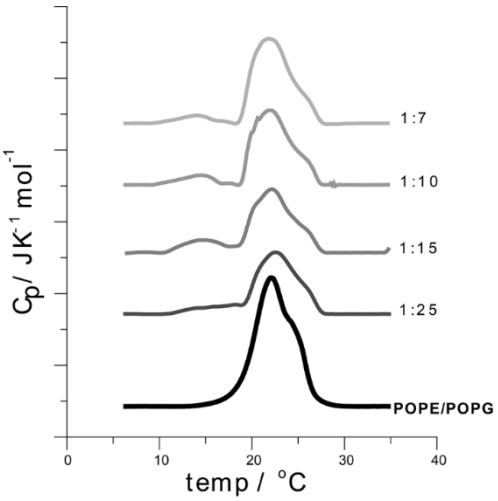

Figure 5 – DSC curves for OLVs of POPE/POPG 3:1 and their mixtures with CAM at different P:L molar ratios. The lipid concentration was 3 mM. Curves are shifted on the y-axis for more clear view of each DSC thermogram, the respective P:L molar ratios are identified for each curve in the figure.

Circular Dichroism

The secondary structure of CAM was examined by Circular Dichroism (CD) in PBS buffer (9.3 mM PBS + 150 mM NaF) and in presence of LUVs of POPE/POPG 3:1 (mol/mol) (Figure 6). Measurements at different peptide concentrations in buffer show that the peptide structure is not affected by concentration (data not shown). For the peptide in presence of the membrane, the results at different P:L ratios were similar. In buffer, the peptide assumes no regular structure (minimum at 198 nm), whereas in presence of POPE/POPG 3:1 a α-helix structure is adopted, with well-defined minima around 208 and 222 nm (Figure 6). The fraction of α-helix was calculated [55] to be 0.33, *i.e.*, only ~5 amino acids are involved in the helix.

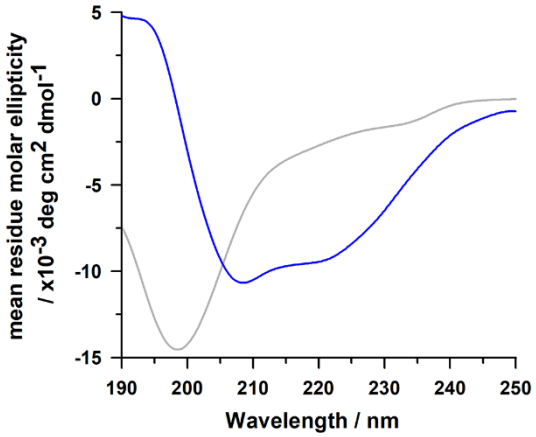

Figure 6 – CD spectra of CAM in buffer (25 μM) (grey) and in a mixture with POPE/POPG (LUVs) 3:1 (3 mM) at P:L=1:50 (blue), at 35 °C.

Isothermal Titration Calorimetry

ITC was used to follow the interaction between CAM and POPE/POPG (LUVs) 3:1 at different temperatures, namely at 30 °C (lipid in L_α phase), at 5 °C (lipid in gel phase) and at 17 °C, a temperature in a range where from the discussion above, we know we have the co-existence of three phases – the L_γ phase, the other phase that appears at low temperature and high peptide contents, and possibly L_α phase, as shown by the DSC and SAXD results (Figure S1 and S5).

The experiments at 30 °C (lipid in L_α phase) show a simple profile with an endothermic effect that drops to zero after a relatively small number of injections (Figures 7A and S6A). Even at the lowest peptide concentration (10 or 15 μM) the steep binding isotherms reflect the large membrane affinity of the peptide, as found in similar systems.[56] Attempts to use lower peptide concentration did not produce isotherms that could be analyzed, due to the very small number of observed peaks.

The results are fitted first to a partition model with correction for electrostatic effects according to Gouy-Chapman theory (Figure 8A).[27, 56-58] In this model, the non-Coulombic interactions of a charged peptide with a lipid membrane are described as a partition equilibrium of the peptide between the interfacial aqueous phase (*i.e.*, the aqueous phase adjacent to the membrane surface), and the lipid bilayer phase. This analysis provides values of the intrinsic partition constant, K_p, the molar transfer enthalpy from the

aqueous phase to the bilayer phase, ΔH, and the effective charge of the peptide, z_{eff}, which determines the strength of Coulombic interactions between the peptide and the membrane.

The results obtained from the fitting of independent experiments at 30 °C, where the peptide concentration in the cell was 15 µM and the lipid concentration in the syringe 30 mM (Figure 8A), lead to the average values K_p = (3.2x10^5± 2x10^5) M^{-1}, ΔH = (27 ±5) kJmol^{-1} and z_{eff} = 4.7±0.4. The overall quality of the fitting is acceptable. The partition constant thus obtained agrees with the one previously determined by Time Resolved Fluorescence Spectroscopy,[14] 5.1x10^5 (when transformed to M^{-1} by use of the lipid molar volume). The z_{eff} value found for the effective charge is smaller than the nominal charge (+6), as expected.[59-60]

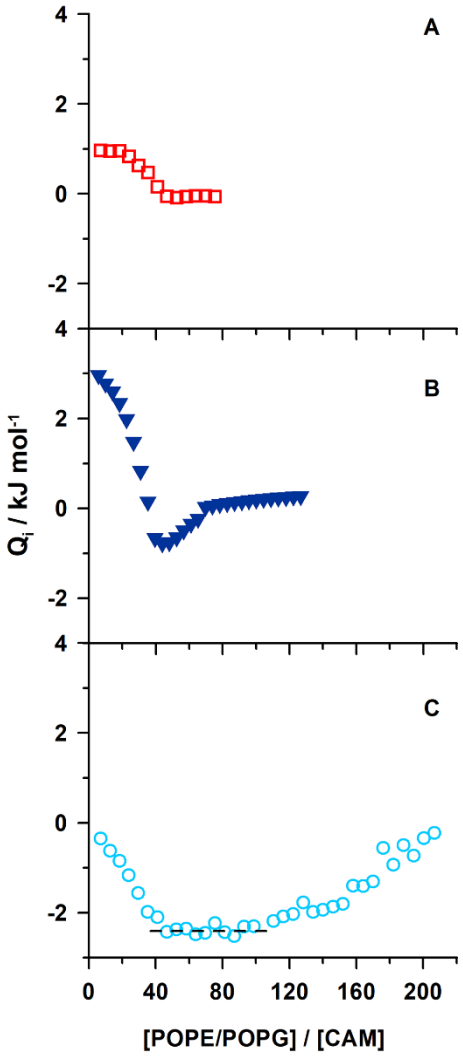

Figure 7 – Integrated peaks as a function of lipid-to-peptide ratio for titration of CAM in buffer (15 μM) with POPE/POPG 3:1 (30 mM) (LUVs) at (A) 30, (B) 17 and (C) 5 °C. The baseline correction and integration were performed using the AFFINImeter software (www.affinimeter.com).

As the curves at 30 °C show a steep binding isotherm (Figure 7A and S6A) we also did the fitting to a binding model, "independent binding sites model" (Figure 8B). As the positively charged peptide has a very strong interaction with the negatively charged bilayer, it is reasonable to try also this model, which has been used recently for AMP/membrane interaction.[61] In fact, the two constants (K_p and K_{app}) can be related, as previously shown,[62-63] and in limiting cases they are similar. The model used provides the microscopy binding constants K_{app} (*i.e.*, per site), the enthalpy change ΔH, and the 'number of sites, n. Thus, the total observed enthalpy can be calculated by multiplying the obtained ΔH by the obtained 'number of sites'. In this treatment we analyzed two sets of data where the peptide concentration in the cell was 15 μM and the titrating lipid suspension was either 15 or 30 mM (see Figure 8B for an example). The retrieved values of the two sets of data agree, yielding the average values $K_{app} = (1.8\text{x}10^5 \pm 0.7\text{x}10^5)$ M^{-1}, $\Delta H = (1.11 \pm 0.02)$ kJmol^{-1} (per site) and number of sites $n = 35 \pm 4$ (thus the total enthalpy observed is 39 ± 5 kJmol^{-1}). The value of n provides information about the extension of the interaction between the lipids and the peptide,[61] indicating that we have ~35 lipids (total lipid content) per peptide. Since the membrane content in POPG is only 25%, this would lead to a total of ~9 POPG per peptide, or about 4.5, if based only on the outer leaflet. Since the interaction of the peptide with the membranes is mostly electrostatically driven, a value similar to that obtained for the effective charge, 4.7, suggests that the peptide interacts only with the outer layer. This is in line with the assumption taken in the partition model calculations where it was assumed that the peptide would only interact with the outer leaflet (γ=0.5). Therefore, within the confines of the difference between the models, we find the agreement satisfactory.

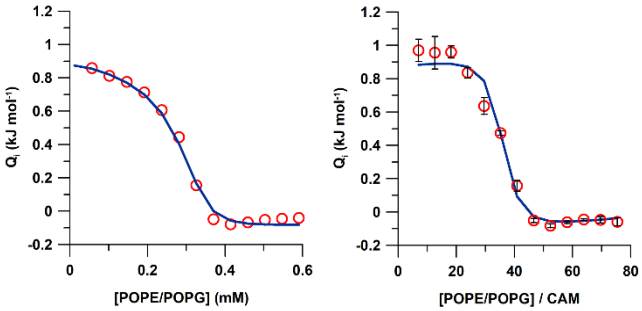

Figure 8 – Titration of CAM (15 μM) with POPE/POPG 3:1 (30 mM) (LUVs) at 30 °C. The integrated reactions heats normalized to the molar amount of injected lipid, Q_i, were obtained with: (A) the NITPIC software and are plotted as a function of lipid concentration in the cell. The data was analyzed by use of a partition model taking into account Coulombic effects according to the Gouy-Chapman theory.[27] (B) AFFINImeter software, and are plotted as a function of lipid-to-peptide ratio in the cell. The data was analyzed using an "independent sites model" (AFFINImeter, www.affinimeter.com). Experimental points are represented by red circles and fitted values by the blue line.

As regarding the experiments at 5 °C, where at least part of the lipid is in the gel phase, a different behavior was observed (figures 7C and S6C). The interaction is exothermic throughout. In the first part of the curve we can see a steep increase in absolute ΔH values up to a P:L ratio of 1:46, followed by a plateau region between 1:46 and 1:87, and thereafter the enthalpy values decreased smoothly towards zero. The initial increase in negative values shows that the peptide/lipid interaction is exothermic in the gel phase, likely reflecting the extensive aggregation of liposomes (or lipid bilayers) induced by the peptide. The fact that the interaction is endothermic at higher and exothermic at lower temperatures indicates that this is not a simple process and that delicate balances among the various interactions (electrostatic, hydrophobic, partial dehydration of the lipid heads upon peptide binding, among others) exist, which are modulated by temperature. It is interesting to observe that at all studied temperatures a similar P:L ratio of ~1:44 (based on total lipid concentration, or 1:22 based on the outer layer) is found

where a change in behavior occurs (Figure 7). Curiously, that value (44) is not far from the *n* value of 35 obtained from the treatment of the isotherms at 35 °C. At 30 °C (Figure 7A), it is the locus where the enthalpy becomes ~zero (only lipid dilution), *i.e.,* the end of the association process. At 17 °C (Figure 7B and S6B), after this point the enthalpy becomes increasingly less negative, approaching the lipid dilution, showing also the end of the interaction process. Finally, at 5 °C (Figure 7C), the onset of a plateau region is observed between P:L ratios of 1:46 and 1:87. Thus we propose that this P:L value is a threshold that reflects lipid saturation by the peptide. The existence of the plateau in the enthalpy values at 5 °C reflects a region after a critical concentration, where phenomena of opposite enthalpy signs occur, or could be a region of coexistence between different phases.[64] Taking into account the interpretation of the interaction given above (see SAXD and SANS results), *i.e*. that the peptide disrupts the membrane forming bilayers stacks intercalated by the peptide, we propose that at this ratio (P:L=1:44) no more free peptide is available to interact with the lipids. Therefore, upon further injection of liposome suspension, the peptide can only redistribute among previous and new lipid layers, what implies disruption of the peptide lipid interaction (endothermic effect at this temperature), followed by association to new lipid layers (exothermic). Indeed, in view of the results discussed above, we suggest that the plateau reflects the formation of another phase, after membrane saturation by the peptide, the one that has a transition at ~14 °C, as we do not know what the value of the onset temperature (we only started the SAXD measurements at 10 °C). Finally, after P:L=1:87 the observed enthalpies only slowly tend to zero.

At intermediate temperatures, 17 °C (Figure 7B and S6B) the ITC curve starts at endothermic values, crosses zero at P:L=1:35 and becomes increasingly negative up to P:L ratio of 1:44 after which it decreases (in absolute value) towards zero (Figure 7B). Thus, the profile is a mixture of those observed at higher (30 °C) and lower (5 °C) temperatures. From the discussion above, at this temperature range we have the co-existence of three phases – the L_{γ} phase, the other phase that appears at low temperature and high peptide contents, and possibly L_{α} phase, as shown by the DSC and SAXD results (Figure S1), resulting in

554 a complex interpretation. In the initial region of excess peptide, we interpret the positive values as
555 reflecting the interaction with the L_α phase (endothermic). Since we have phases in equilibrium, this can
556 induce some phase transition (endothermic) to the L_α phase, justifying that for the same P:L ratios the
557 observed enthalpy values are more positive than those encountered at 30 °C. Indeed, this increase can also
558 result from a change in enthalpy with temperature. Beyond P:L=1:35 the negative values must reflect the
559 interaction with the part of the system that is in gel phase, up to saturation at P:L=1:44. Finally beyond
560 the critical P:L ratio of 1:44, there is a large excess of lipid and the values decrease towards zero, as
561 observed at the other studied temperatures.

562 Finally we want to point out that the critical P:L ratio where a minimum in the enthalpy profiles occurs
563 for all studied temperatures (around 1:44) is similar to that found by Bhargava and Feix in a EPR study
564 of the interaction of this peptide with POPE/POPG 80:20.[65]

565 **Fluorescence microscopy**

566 In order to further investigate the mechanism of action of CAM on POPE/POPG 3:1 membranes, and
567 to shed light onto the formed structures, we perform fluorescence microscopy using OLVs of
568 POPE/POPG 3:1 (mol/mol) labelled with Texas Red®-DHPE. Three different samples were visualized,
569 the pure lipid mixture and two peptide/lipid mixtures at P:L of 1:25 and 1:10 (Figure 9). The pure lipid
570 mixture shows, as expected, oligolamellar vesicles of different sizes, well dispersed in the support (Figure
571 9A). The mixtures present a completely different structure, with very large aggregates for both P:L ratios
572 (Figure 9B,C,D,E). This is in line with the hypothesis of the peptide inducing extensive aggregation of
573 the lipid system, supported by our SANS, SAXD and DSC results. Although in both cases an extensive
574 aggregation is apparent, at the highest P:L ratio significantly larger aggregates are observed (Figure 9C,E),
575 whereas a bridged network between smaller structures appears at P:L=1:25 (Figure 9B,D).

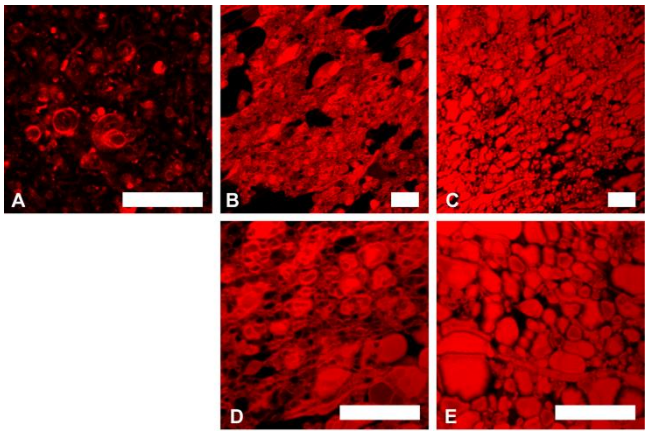

Figure 9 – Fluorescence confocal microscopy of POPE/POPG 3:1 (OLVs) containing 0.3% of Texas Red®-DHPE and its mixture with CAM at different P:L ratios, at 35 °C. Upper panel: (A) POPE/POPG 3:1; (B) P:L=1:25; (C) P:L=1:10. Lower panel: same mixtures as in the upper panel but at higher magnification: (D) P:L=1:25; (E) P:L=1:10. Scale bar: 15 μm.

Electron Microscopy

The use of negative staining electron microscopy provides some complementary information of the structural characteristics of mixtures of CAM and LUVs of POPE/POPG 3:1. The system was studied at a temperature below T_m and for different P:L ratios (1:25 and 1:10). Some tests were also performed above T_m with poor results (data not shown) - no identifiable structures could be detected, as neither vesicle structures nor lamellar stacks could be clearly seen.

For the temperature below T_m, in the case of pure lipid mixture individual spherical vesicles are observed, revealing the presence of liposomes (Figure 10A). When the peptide is added, condensation occurs, with large aggregates being formed by multilamellar or disrupted vesicles (Figure 10 B,C,D), in agreement with the observations by fluorescence microscopy (Figure 10). The aggregates are larger in the sample with higher peptide content at 1:10 as compared to 1:25 (Figure 10 C,B respectively), also in line with the observations by fluorescence microscopy (Figure 9). In the enlargement presented in Figure 10 D we can easily see the different layers of the “onion like” structure.

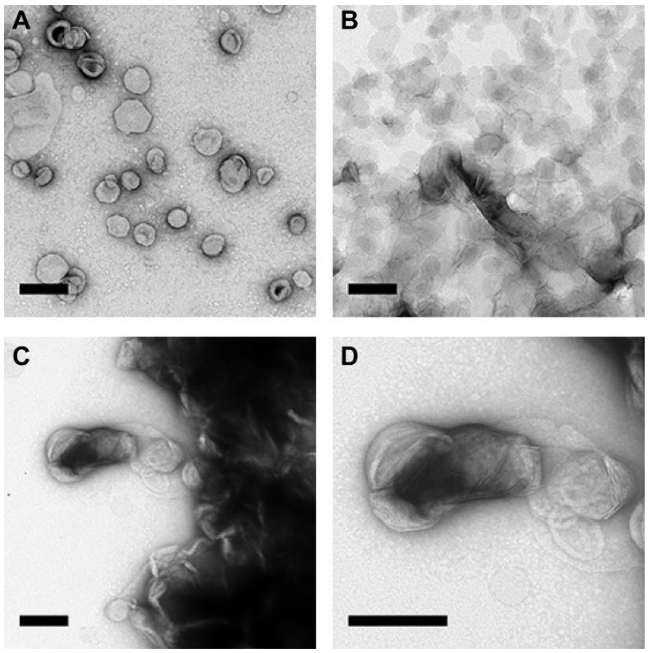

Figure 10 – Negative staining electron microscopy of POPE/POPG 3:1 (LUVs) and its mixture with CAM at different P:L ratios. Samples were incubated below T_m, in the gel state (~4 °C). (A) POPE/POPG 3:1; (B) P:L=1:25; (C) P:L=1:10; (D) higher magnification of C. Scale bar: 250 nm.

Conclusions

The system CAM-POPE/POPG 3:1 was studied by a large number of techniques, in order to unravel the mode of interaction of this peptide with a model membrane system and understand its antimicrobial mechanism of action.

The obtained results are consistent, and lead us to propose that CAM interacts strongly with the negatively charged membrane system, destroying the liposomes and leading to a lamellar stack of multilayers with peptide intercalated between them, in an onion-like structure. This behavior is similar to the condensation observed in CL-DNA systems, widely described in the literature.[48, 66-67] This is clearly shown by SANS, where the increase in the number of layers upon peptide addition supports this suggestion. Further, the results obtained by SAXD are compatible with the formation of a L_γ phase in the presence of the peptide, what reconciles the observed reversibility upon up and down temperature scans

610 and the large difference in periodicities retrieved at high and low temperatures. To the best of our
611 knowledge, this phase has not been reported in this context. DSC results also support the formation of
612 multilayers, as reflected by the increased cooperativity of the main transition. Further, they clearly show
613 the presence of another phase at lower temperatures, the relative proportion of which increases with
614 peptide content, consistently with SAXD results. Finally, the fluorescence and electron microscopy results
615 show the large difference between the pure lipid and the combined peptide/lipid system, in structures
616 compatible to the proposed aggregation/condensation.

617 A study by Ladokhin and White [68] showed that whereas melittin (a related peptide, as CAM is a cecropin
618 A-melittin hybrid) induces leakage through pores of about 25 Å diameter in zwitterionic membranes,[69]
619 leakage from POPG vesicles is non-selective, *i.e.*, 'detergent-like' or implying liposome destruction.[68]
620 These results are consistent with our findings, as the mechanism we propose leads to liposome destruction
621 and not to pore formation.

622 Finally, the ITC results show that the enthalpy of interaction is endothermic in the L_α phase and
623 exothermic at lower temperatures. Further, at high P:L ratios and temperatures of coexistence of different
624 phases, the peptide probably induces a phase transition. In all cases a threshold P:L ratio of 1:44 is found,
625 which we interpret as a saturation concentration. Moreover, the obtained fitted value of n in the L_α phase
626 (~35 lipids per peptide) is comparable to the threshold value of 1:44, providing information on the extent
627 of interaction between lipids and peptide.[61] This value is expected, knowing that the calculated effective
628 charge is around 4, assuming that the peptide only interacts with the outer lipid leaflet. This result is again
629 in line with the peptide interaction at the level of the phospholipid headgroups, inducing membrane
630 condensation beyond a threshold value (related to charge neutralization) and not pore formation. We are
631 aware that pore formation induced by CAM has been reported for other systems,[15, 17, 19] but our results for
632 the POPE/POPG lipid system are not compatible with the same mechanism, confirming that the

633 mechanism of action of antimicrobial peptides depends not only on the peptide, but on lipid membrane
634 system as well.[70-71]

635 Since the system studied in this work is a good model of a bacterial membrane, where PE and PG are
636 the most abundant phospholipids,[21] and this peptide has proven antimicrobial action,[8, 10] the mechanism
637 proposed here could be intrinsic to its mechanism of action, because it potentially leads to bacterial
638 membrane destruction, loss of membrane potential and inner contents, ultimately leading to cell death.
639

640 ASSOCIATED CONTENT

641 **Supporting Information**. Detailed description of sample preparation and handling for SANS, SAXD,
642 DSC and Electron Microscopy. Dependence of lattice parameters on temperature, for the different phases
643 of POPE, POPE/POPG 3:1, and mixtures with CAM at several P:L ratios. SAXD patterns of selected
644 samples taken at temperature scans. Analysis of SAXD peaks in respect to lamellae fluctuations. WAXD
645 patterns of selected samples. Decomposition of DSC curves for CAM-POPE/POPG P:L=1:10. Raw ITC
646 curves at the three reported temperatures. This material is available free of charge via the internet at
647 http://pubs.acs.org.

648 AUTHOR INFORMATION

649 **Corresponding authors**

650 * Margarida Bastos, e-mail: mbastos@fc.up.pt; * Daniela Uhríková, e-mail: uhrikova@fpharm.uniba.sk

651 **Acknowledgements**

652 The authors thank Lukáš Hubčík for his help at SAXD experiments. MB, TS and BFBS would like to
653 thank Cyrus Safinya for earlier discussions on the interpretation of the data. MB and TS would like to
654 thank Sandro Keller for kindly providing his software to perform ITC partition data analysis, and Johannes

655 Klinger for support and advice on error analysis. The research received support from grants NORTE-07-
656 0162-FEDER-000088 of the Programa Operacional Regional do Norte (ON.2 – O Novo Norte) funded
657 by Fundo Europeu de Desenvolvimento Regional (Feder), NORTE-01-0145-FEDER-000028,
658 Sustainable Advanced Materials (SAM), Programa Operacional Regional do Norte (Norte 2020), awarded
659 to CIQ-UP, strategic projects Pest-C/QUI/UI0081/2011 and Pest-C/QUI/UI0081/2013 from Fundação
660 para a Ciência e Tecnologia (FCT) and European Social Funds, to CIQ-UP; PhD grant
661 SFRH/BD/77564/2011 from FCT to TS and PD/BD/135095/2017 to BC; FCT for financial support to
662 LAQV/REQUIMTE (UID/QUI/50006/2013) and IF position and IF/00092/2014 project to NV; EC's 7th
663 Framework Program (FP7/2007-2013) under grant agreement no. 226716 (HASYLAB project II-
664 20090024 EC); SK-PT-0015-10 to DU, MB and TS; VEGA 1/0916/16 to DU. SANS experiment (LLB
665 11046) was supported by the EC under the 7th FP: Strengthening the European Research Area, Research
666 Infrastructures, Contract NMI3-II/FP7 No 283883. This work benefited from the use of the SasView
667 application, originally developed under NSF award DMR-052547. SasView contains code developed with
668 funding from the European Union's Horizon 2020 research and innovation program under the SINE2020
669 project, grant agreement No 654000.

670

671 REFERENCES

672 (1) Bassetti, M.; Merelli, M.; Temperoni, C.; Astilean, A. New antibiotics for bad bugs: where are we?
673 *Ann. Clin. Microbiol. Antimicrob.* **2013,** *12*, 22.

674 (2) Fischbach, M. A.; Walsh, C. T. Antibiotics for emerging pathogens. *Science* **2009,** *325*, 1089-93.

675 (3) Yeung, A.; Gellatly, S.; Hancock, R. Multifunctional cationic host defence peptides and their clinical
676 applications. *Cell Mol. Life Sci.* **2011,** *68*, 2161-2176.

677 (4) Nguyen, L. T.; Haney, E. F.; Vogel, H. J. The expanding scope of antimicrobial peptide structures and
678 their modes of action. *Trends Biotechnol.* **2011,** *29*, 464-472.

679 (5) Mansour, S. C.; Pena, O. M.; Hancock, R. E. Host defense peptides: front-line immunomodulators.
680 *Trends Immunol.* **2014,** *35*, 443-50.

(6) Haney, E. F.; Hancock, R. E. Peptide design for antimicrobial and immunomodulatory applications. *Biopolymers* **2013,** *100*, 572-83.

(7) Brogden, N. K.; Brogden, K. A. Will new generations of modified antimicrobial peptides improve their potential as pharmaceuticals? *Int. J. Antimicrob. Agents* **2011,** *38*, 217-25.

(8) Boman, H. G.; Wade, D.; Boman, I. A.; Wahlin, B.; Merrifield, R. B. Antibacterial and antimalarial properties of peptides that are cecropin-melittin hybrids. *FEBS Lett.* **1989,** *259*, 103-6.

(9) Wade, D.; Boman, A.; Wahlin, B.; Drain, C. M.; Andreu, D.; Boman, H. G.; Merrifield, R. B. All-D amino acid-containing channel-forming antibiotic peptides. *Proc. Natl. Acad. Sci. U. S. A.* **1990,** *87*, 4761-5.

(10) Andreu, D.; Ubach, J.; Boman, A.; Wahlin, B.; Wade, D.; Merrifield, R. B.; Boman, H. G. Shortened cecropin A-melittin hybrids. Significant size reduction retains potent antibiotic activity. *FEBS Lett.* **1992,** *296*, 190-4.

(11) Abrunhosa, F.; Faria, S.; Gomes, P.; Tomaz, I.; Pessoa, J. C.; Andreu, D.; Bastos, M. Interaction and Lipid-Induced Conformation of Two Cecropin−Melittin Hybrid Peptides Depend on Peptide and Membrane Composition. *J. Phys. Chem. B* **2005,** *109*, 17311-17319.

(12) Bastos, M.; Bai, G.; Gomes, P.; Andreu, D.; Goormaghtigh, E.; Prieto, M. Energetics and partition of two cecropin-melittin hybrid peptides to model membranes of different composition. *Biophys. J.* **2008,** *94*, 2128-41.

(13) Diaz-Achirica, P.; Prieto, S.; Ubach, J.; Andreu, D.; Rial, E.; Rivas, L. Permeabilization of the mitochondrial inner membrane by short cecropin-A-melittin hybrid peptides. *Eur. J. Biochem.* **1994,** *224*, 257-63.

(14) Teixeira, V.; Feio, M. J.; Rivas, L.; De la Torre, B. G.; Andreu, D.; Coutinho, A.; Bastos, M. Influence of Lysine Nε-Trimethylation and Lipid Composition on the Membrane Activity of the Cecropin A-Melittin Hybrid Peptide CA(1−7)M(2−9). *J. Phys. Chem. B* **2010,** *114*, 16198-16208.

(15) Milani, A.; Benedusi, M.; Aquila, M.; Rispoli, G. Pore forming properties of cecropin-melittin hybrid peptide in a natural membrane. *Molecules* **2009,** *14*, 5179-88.

(16) Pistolesi, S.; Pogni, R.; Feix, J. B. Membrane insertion and bilayer perturbation by antimicrobial peptide CM15. *Biophys. J.* **2007,** *93*, 1651-60.

(17) Sato, H.; Feix, J. B. Osmoprotection of bacterial cells from toxicity caused by antimicrobial hybrid peptide CM15. *Biochemistry* **2006,** *45*, 9997-10007.

(18) Diaz-Achirica, P.; Ubach, J.; Guinea, A.; Andreu, D.; Rivas, L. The plasma membrane of Leishmania donovani promastigotes is the main target for CA(1-8)M(1-18), a synthetic cecropin A-melittin hybrid peptide. *Biochem. J.* **1998,** *330 (Pt 1)*, 453-60.

(19) Juvvadi, P.; Vunnam, S.; Merrifield, E. L.; Boman, H. G.; Merrifield, R. B. Hydrophobic effects on antibacterial and channel-forming properties of cecropin A-melittin hybrids. *J. Pept. Sci.* **1996,** *2*, 223-32.

(20) Ferre, R.; Melo, M. N.; Correia, A. D.; Feliu, L.; Bardaji, E.; Planas, M.; Castanho, M. Synergistic effects of the membrane actions of cecropin-melittin antimicrobial hybrid peptide BP100. *Biophys. J.* **2009,** *96*, 1815-27.

(21) Teixeira, V.; Feio, M. J.; Bastos, M. Role of lipids in the interaction of antimicrobial peptides with membranes. *Prog. Lipid Res.* **2012,** *51*, 149-177.

(22) Fernandez-Reyes, M.; Diaz, D.; de la Torre, B. G.; Cabrales-Rico, A.; Valles-Miret, M.; Jimenez-Barbero, J.; Andreu, D.; Rivas, L. Lysine N(epsilon)-trimethylation, a tool for improving the selectivity of antimicrobial peptides. *J. Med. Chem.* **2010,** *53*, 5587-96.

(23) Silva, T.; Adao, R.; Nazmi, K.; Bolscher, J. G.; Funari, S. S.; Uhrikova, D.; Bastos, M. Structural diversity and mode of action on lipid membranes of three lactoferrin candidacidal peptides. *Biochim Biophys Acta* **2013,** *1828*, 1329-39.

(24) Huang, T. C.; Toraya, H.; Blanton, T. N.; Wu, Y. X-ray powder diffraction analysis of silver behenate, a possible low-angle diffraction standard. *J. Appl. Cryst.* **1993,** *26*, 180-184.

(25) Roveri, N.; Bigi, A.; Castellani, P. P.; Foresti, E.; Marchini, M.; Strocchi, R. [Study of rat tail tendon by x-ray diffraction and freeze-etching technics]. *Boll. - Soc. Ital. Biol. Sper.* **1980,** *56*, 953-9.

(26) Keller, S.; Vargas, C.; Zhao, H.; Piszczek, G.; Brautigam, C. A.; Schuck, P. High-precision isothermal titration calorimetry with automated peak-shape analysis. *Anal Chem.* **2012,** *84*, 5066-73.

(27) Vargas, C.; Klingler, J.; Keller, S. Membrane partitioning and translocation studied by isothermal titration calorimetry. *Methods Mol. Biol.* **2013,** *1033*, 253-71.

(28) Meister, A.; Finger, S.; Hause, G.; Blume, A. Morphological changes of bacterial model membrane vesicles. *Eur. J. Lipid Sci. Technol.* **2014,** *116*, 1228-1233.

(29) Bergström, M.; Pedersen, J. S.; Schurtenberger, P.; Egelhaaf, S. U. Small-Angle Neutron Scattering (SANS) Study of Vesicles and Lamellar Sheets Formed from Mixtures of an Anionic and a Cationic Surfactant. *J. Phys. Chem. B* **1999,** *103*, 9888-9897.

(30) DMR-0520547, S.-D. p. u. N. a. SasView. http://www.sasview.org/ (accessed March 2017).

(31) Uhríková, D.; Teixeira, J.; Hubčík, L.; Búcsi, A.; Kondela, T.; Murugova, T.; Ivankov, O. I. Lipid based drug delivery systems: Kinetics by SANS. *Journal of Physics: Conference Series* **2017,** *848*, 012007.

(32) Kučerka, N.; van Oosten, B.; Pan, J.; Heberle, F. A.; Harroun, T. A.; Katsaras, J. Molecular Structures of Fluid Phosphatidylethanolamine Bilayers Obtained from Simulation-to-Experiment Comparisons and Experimental Scattering Density Profiles. *J. Phys. Chem. B* **2015,** *119*, 1947-1956.

(33) Pan, J.; Heberle, F. A.; Tristram-Nagle, S.; Szymanski, M.; Koepfinger, M.; Katsaras, J.; Kučerka, N. Molecular structures of fluid phase phosphatidylglycerol bilayers as determined by small angle neutron and X-ray scattering. *Biochim. Biophys. Acta* **2012,** *1818*, 2135-2148.

(34) Pozo Navas, B.; Lohner, K.; Deutsch, G.; Sevcsik, E.; Riske, K. A.; Dimova, R.; Garidel, P.; Pabst, G. Composition dependence of vesicle morphology and mixing properties in a bacterial model membrane system. *Biochim. Biophys. Acta* **2005,** *1716*, 40-8.

(35) Pandit, K. R.; Klauda, J. B. Membrane models of E. coli containing cyclic moieties in the aliphatic lipid chain. *Biochim. Biophys. Acta* **2012,** *1818*, 1205-1210.

(36) Kučerka, N.; Holland, B. W.; Gray, C. G.; Tomberli, B.; Katsaras, J. Scattering Density Profile Model of POPG Bilayers As Determined by Molecular Dynamics Simulations and Small-Angle Neutron and X-ray Scattering Experiments. *J. Phys. Chem. B* **2012,** *116*, 232-239.

(37) Nallet, F.; Laversanne, R.; Roux, D. Modelling X-ray or neutron scattering spectra of lyotropic lamellar phases : interplay between form and structure factors. *J. Phys. II France* **1993,** *3*, 487-502

(38) Caillè, A. *C. R. Acad. Sci. Paris B* **1972,** *274*, 1733.

(39) Petrache, H. I.; Gouliaev, N.; Tristram-Nagle, S.; Zhang, R.; Suter, R. M.; Nagle, J. F. Interbilayer interactions from high-resolution x-ray scattering. *Phys. Rev. E* **1998,** *57*, 7014 – 7024.

(40) Pabst, G.; Grage, S. L.; Danner-Pongratz, S.; Jing, W.; Ulrich, A. S.; Watts, A.; Lohner, K.; Hickel, A. Membrane Thickening by the Antimicrobial Peptide PGLa. *Biophys. J.* **2008,** *95*, 5779-5788.

(41) Lee, M. T.; Chen, F. Y.; Huang, H. W. Energetics of pore formation induced by membrane active peptides. *Biochemistry* **2004,** *43*, 3590-9.

(42) Lee, J.-H.; Choi, S.-M.; Doe, C.; Faraone, A.; Pincus, P. A.; Kline, S. R. Thermal Fluctuation and Elasticity of Lipid Vesicles Interacting with Pore-Forming Peptides. *Phys. Rev. Lett.* **2010,** *105*, 038101.

(43) Pabst, G.; Danner, S.; Podgornik, R.; Katsaras, J. Entropy-Driven Softening of Fluid Lipid Bilayers by Alamethicin. *Langmuir* **2007,** *23*, 11705-11711.

(44) Vitkova, V.; Méléard, P.; Pott, T.; Bivas, I. Alamethicin influence on the membrane bending elasticity. *Eur. Biophys. J.* **2006,** *35*, 281-286.

(45) Domingues, M. M.; Bianconi, M. L.; Barbosa, L. R. S.; Santiago, P. S.; Tabak, M.; Castanho, M. A. R. B.; Itri, R.; Santos, N. C. rBPI21 interacts with negative membranes endothermically promoting the formation of rigid multilamellar structures. *Biochim. Biophys. Acta* **2013,** *1828*, 2419-2427.

(46) Nagle, J. F.; Tristram-Nagle, S. Structure of lipid bilayers. *Biochim. Biophys. Acta, Rev. Biomembr.* **2000,** *1469*, 159-195.

(47) May, S.; Ben-Shaul, A. Modeling of Cationic Lipid-DNA Complexes. *Curr. Med. Chem.* **2004,** *11*, 151-167.

(48) Rädler, J. O.; Koltover, I.; Salditt, T.; Safinya, C. R. Structure of DNA-Cationic Liposome Complexes: DNA Intercalation in Multilamellar Membranes in Distinct Interhelical Packing Regimes. *Science* **1997,** *275*, 810-814.

(49) Uhríková, D.; Hanulová, M.; Funari, S. S.; Lacko, I.; Devínsky, F.; Balgavý, P. The structure of DNA–DLPC–cationic gemini surfactant aggregates: a small angle synchrotron X-ray diffraction study. *Biophys. Chem.* **2004,** *111*, 197-204.

(50) Gulik, A.; Tchoreloff, P.; Proust, J. A conformation transition of lung surfactant lipids probably involved in respiration. *Biophys. J.* **1994,** *67*, 1107-12.

(51) Mateu, L.; Luzzati, V.; London, Y.; Gould, R. M.; Vosseberg, F. G. A.; Olive, J. X-ray diffraction and electron microscope study of the interactions of myelin components. The structure of a lamellar phase with a 150 to 180 Å repeat distance containing basic proteins and acidic lipids. *J. Mol. Biol.* **1973,** *75*, 697-709.

(52) Ranck, J. L.; Mateu, L.; Sadler, D. M.; Tardieu, A.; Gulik-Krzywicki, T.; Luzzati, V. Order-disorder conformational transitions of the hydrocarbon chains of lipids. *J. Mol. Biol.* **1974,** *85*, 249-77.

(53) Ranck, J. L.; Zaccai, G.; Luzzati, V. The structure of a lipid-water lamellar phase containing two types of lipid monolayers. An X-ray and neutron scattering study. *J. Appl. Crystallog.* **1980,** *13*, 505-512.

(54) Funari, S. S.; Rapp, G.; Richter, F. Double-bilayer: a new phase formed by lysophospholipids and the corresponding fatty acid. *Quim. Nova* **2009,** *32*, 908-912.

(55) Ladokhin, A. S.; White, S. H. Folding of amphipathic alpha-helices on membranes: energetics of helix formation by melittin. *J. Mol. Biol.* **1999,** *285*, 1363-9.

(56) Scheidt, H. A.; Klingler, J.; Huster, D.; Keller, S. Structural Thermodynamics of myr-Src(2-19) Binding to Phospholipid Membranes. *Biophys. J.* **2015,** *109*, 586-94.

(57) Seelig, J. Thermodynamics of lipid-peptide interactions. *Biochim. Biophys. Acta* **2004,** *1666*, 40-50.

(58) Martins, P. T.; Velazquez-Campoy, A.; Vaz, W. L.; Cardoso, R. M.; Valerio, J.; Moreno, M. J. Kinetics and thermodynamics of chlorpromazine interaction with lipid bilayers: effect of charge and cholesterol. *J Am Chem Soc* **2012,** *134*, 4184-95.

(59) Klocek, G.; Schulthess, T.; Shai, Y.; Seelig, J. Thermodynamics of Melittin Binding to Lipid Bilayers. Aggregation and Pore Formation. *Biochemistry* **2009,** *48*, 2586-2596.

(60) Scheidt, Holger A.; Klingler, J.; Huster, D.; Keller, S. Structural Thermodynamics of myr-Src(2–19) Binding to Phospholipid Membranes. *Biophys. J.* **2015,** *109*, 586-594.

(61) Arouri, A.; Dathe, M.; Blume, A. The helical propensity of KLA amphipathic peptides enhances their binding to gel-state lipid membranes. *Biophys. Chem.* **2013,** *180-181*, 10-21.

(62) Bastos, M.; Castro, V.; Mrevlishvili, G.; Teixeira, J. Hydration of ds-DNA and ss-DNA by neutron quasielastic scattering. *Biophys. J.* **2004,** *86*, 3822-7.

(63) Melo, M. N.; Ferre, R.; Feliu, L.; Bardaji, E.; Planas, M.; Castanho, M. A. Prediction of antibacterial activity from physicochemical properties of antimicrobial peptides. *PLoS One* **2011,** *6*, e28549.

(64) Garidel, P.; Hildebrand, A.; Knauf, K.; Blume, A. Membranolytic activity of bile salts: influence of biological membrane properties and composition. *Molecules* **2007,** *12*, 2292-326.

(65) Bhargava, K.; Feix, J. B. Membrane binding, structure, and localization of cecropin-mellitin hybrid peptides: a site-directed spin-labeling study. *Biophys. J.* **2004,** *86*, 329-36.

(66) Bouxsein, N. F.; Leal, C.; McAllister, C. S.; Ewert, K. K.; Li, Y.; Samuel, C. E.; Safinya, C. R. Two-dimensional packing of short DNA with nonpairing overhangs in cationic liposome-DNA complexes: from Onsager nematics to columnar nematics with finite-length columns. *J. Am. Chem. Soc.* **2011,** *133*, 7585-95.

(67) Koltover, I.; Salditt, T.; Rädler, J. O.; Safinya, C. R. An Inverted Hexagonal Phase of Cationic Liposome-DNA Complexes Related to DNA Release and Delivery. *Science* **1998,** *281*, 78-81.

(68) Ladokhin, A. S.; White, S. H. 'Detergent-like' permeabilization of anionic lipid vesicles by melittin. *Biochim. Biophys. Acta* **2001,** *1514*, 253-60.

(69) Ladokhin, A. S.; Selsted, M. E.; White, S. H. Sizing membrane pores in lipid vesicles by leakage of co-encapsulated markers: pore formation by melittin. *Biophys. J.* **1997,** *72*, 1762-6.

(70) Arouri, A.; Kerth, A.; Dathe, M.; Blume, A. The Binding of an Amphipathic Peptide to Lipid Monolayers at the Air/Water Interface Is Modulated by the Lipid Headgroup Structure. *Langmuir* **2011,** *27*, 2811-2818.

(71) Lu, J.-x.; Blazyk, J.; Lorigan, G. A. Exploring membrane selectivity of the antimicrobial peptide KIGAKI using solid-state NMR spectroscopy. *Biochim. Biophys. Acta* **2006,** *1758*, 1303-1313.

837 **Table of Contents Graphic**

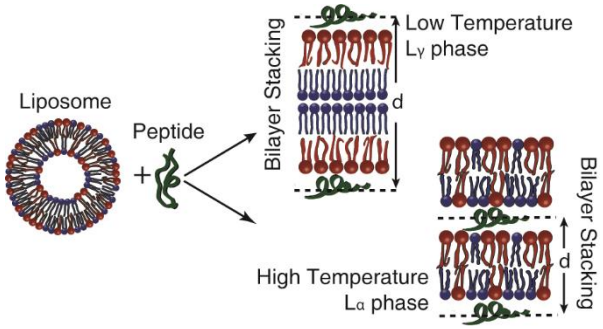

838

839

840

841

842

843